

Tomography of entangled massive particles

C. F. Roos, G. P. T. Lancaster, M. Riebe, H. Häffner, W. Hänsel,

S. Gulde, C. Becher, J. Eschner, F. Schmidt-Kaler and R. Blatt

Institut für Experimentalphysik, Universität Innsbruck, Technikerstrasse 25, A-6020 Innsbruck, Austria

(Dated: October 30, 2018)

We report on tomographic means to study the stability of a qubit register based on a string of trapped ions. In our experiment, two ions are held in a linear Paul trap and are entangled deterministically by laser pulses that couple their electronic and motional states. We reconstruct the density matrix using single qubit rotations and subsequent measurements with near-unity detection efficiency. This way, we characterize the created Bell states, the states into which they subsequently decay, and we derive their entanglement, applying different entanglement measures.

PACS numbers: PACS number(s): 03.65.Ud, 03.67.Mn

Quantum state tomography[1] allows the estimation of an unknown quantum state that is available in many identical copies. It has been experimentally demonstrated for a variety of physical systems, among them the quantum state of a light mode[2], the vibrational state of a molecule[3] and a single ion[4], and the wave packets of atoms of an atomic beam[5]. Multi-particle states have been investigated in nuclear magnetic resonance experiments[6] as well as in experiments involving entangled photon pairs[7, 8]. However, no experiment to date has completely reconstructed the quantum state of entangled massive particles [9, 10, 11, 12]. In the context of quantum information theory[13], multi-particle entangled states are considered to be an essential resource for processing information encoded in quantum states (qubits). Many protocols require the deterministic creation of entangled states and the preservation of these states over times much longer than their production time. For experiments aiming at entangling qubits, the coupling of the qubits to the environment needs to be well understood so that its effect can be minimized.

In this article, we describe the deterministic creation of all four two-ion Bell states, i.e. $\Psi_{\pm} = (|10\rangle \pm |01\rangle)/\sqrt{2}$ and $\Phi_{\pm} = (|11\rangle \pm |00\rangle)/\sqrt{2}$, where $|x_1 x_2\rangle$, $x_i \in \{0, 1\}$ represents the combined state of the two qubits. By tomographically reconstructing the two-ion density matrix, we fully characterize these states and determine their entanglement by different means. We also measure the time evolution of these states and determine the decay of their entanglement.

In our experiments, a qubit is encoded in a superposition of internal states of a calcium ion. We use the $|S_{1/2}, m = -1/2\rangle$ ground state and the metastable $|D_{5/2}, m = -1/2\rangle$ state (lifetime $\tau \sim 1$ s) to represent the qubit states $|1\rangle$ and $|0\rangle$, respectively. Two $^{40}\text{Ca}^+$ ions are loaded into a linear Paul trap having vibrational frequencies of $(2\pi)1.2$ MHz in the axial and $(2\pi)5$ MHz in the transverse directions. After 10 ms of Doppler and sideband cooling [14], the ions' breathing mode of axial vibration at $\omega_b = (2\pi)\sqrt{3} \times 1.2$ MHz is cooled to the ground state $|0_b\rangle$ (99% occupation). Thereafter, the qubits are

initialized in the $|11\rangle$ state. For quantum state engineering, we employ a narrowband Ti:Sapphire laser which is tightly focussed onto either one of the two ions. By exciting the $S_{1/2}$ to $D_{5/2}$ quadrupole transition near 729 nm ($\gamma = 0.16$ Hz), we prepare a single ion in a superposition of the $|0\rangle$ and $|1\rangle$ states. If the laser excites the transition on resonance ("carrier transition"), the ion's vibrational state is not affected whereas if the laser frequency is set to the transition's upper motional sideband ("blue sideband"), the electronic states become entangled with the motional states $|0_b\rangle$ and $|1_b\rangle$ of the breathing mode. We use an acousto-optical modulator to switch between carrier and sideband transition frequency and to control the phase of the light field [12, 14, 15, 16]. An electro-optical beam deflector switches the laser beam from one ion, over a distance of $5.3 \mu\text{m}$, to the other ion within $15 \mu\text{s}$. Directing the beam which has a width of $2.5 \mu\text{m}$ (FWHM at the focus) onto one ion, the intensity on the neighboring ion is suppressed by a factor of $2.5 \cdot 10^{-3}$. By a sequence of laser pulses of appropriate length, frequency, and phase, the two ions are prepared in a Bell state as described below. For detection of the internal quantum states, we excite the $S_{1/2}$ to $P_{1/2}$ dipole transition near 397 nm and monitor the fluorescence for 15 ms with an intensified CCD camera separately for each ion. Fluorescence indicates that the ion was in the $S_{1/2}$ state, no fluorescence reveals that it was in the $D_{5/2}$ state. By repeating the experimental cycle 200 times we find the average populations of all product basis states $|00\rangle$, $|01\rangle$, $|10\rangle$ and $|11\rangle$.

We create a Bell state by applying laser pulses to ion 1 and 2 on the blue sideband and the carrier. Using the Pauli spin matrices $\sigma_x, \sigma_y, \sigma_z$ [17] and the operators b and b^\dagger that annihilate and create a phonon in the breathing mode, we denote single qubit carrier rotations of qubit α by

$$R_\alpha(\theta, \phi) = \exp \left[i \frac{\theta}{2} \left(\sigma_x^{(\alpha)} \cos \phi - \sigma_y^{(\alpha)} \sin \phi \right) \right] \quad (1)$$

and rotations on the blue sideband of the vibrational

breathing mode by

$$R_\alpha^+(\theta, \phi) = \exp \left[i \frac{\theta}{2} \left(\sigma_x^{(\alpha)} b^\dagger \cos \phi - \sigma_y^{(\alpha)} b \sin \phi \right) \right]. \quad (2)$$

Now, we produce the Bell state $\Psi_\pm = (|10\rangle \pm |01\rangle)/\sqrt{2}$ by the pulse sequence $U_{\Psi_\pm} = R_2^+(\pi, \pm\pi/2)R_2(\pi, \pi/2)R_1^+(\pi/2, -\pi/2)$ applied to the $|11\rangle$ state. The pulse $R_1^+(\pi/2, -\pi/2)$ entangles the motional and the internal degrees of freedom, the next two pulses $R_2^+(\pi, \pm\pi/2)R_2(\pi, \pi/2)$ map the motional degree of freedom onto the internal state of ion 2. Appending another π -pulse, $U_{\Phi_\pm} = R_2(\pi, 0)U_{\Psi_\pm}$, produces the state Φ_\pm up to a global phase. The pulse sequence takes less than 200 μ s.

To account for experimental imperfections, we describe the quantum state by a density matrix ρ . For its experimental determination we expand ρ into a superposition $\rho = \sum_i \lambda_i O_i$ of mutually orthogonal Hermitian operators O_i , which form a basis and obey the equation $\text{tr}(O_i O_j) = 4\delta_{ij}$ [18]. Then, the coefficients λ_i are related to the expectation values of O_i by $\lambda_i = \text{tr}(\rho O_i)/4$. For a two-qubit system, a convenient set of operators is given by the 16 operators $\sigma_i^{(1)} \otimes \sigma_j^{(2)}$, ($i, j = 0, 1, 2, 3$), where $\sigma_i^{(\alpha)}$ runs through the set of Pauli matrices $1, \sigma_x, \sigma_y, \sigma_z$, of qubit α .

The reconstruction of the density matrix ρ is now accomplished by measuring the expectation values $\langle \sigma_i^{(1)} \otimes \sigma_j^{(2)} \rangle_\rho$. A fluorescence measurement projects the quantum state into one of the states $|x_1 x_2\rangle$, $x_i \in \{0, 1\}$. By repeatedly preparing and measuring the quantum state, we obtain the average population in states $|x_1 x_2\rangle$ from which we calculate the expectation values of $\sigma_z^{(1)}$, $\sigma_z^{(2)}$ and $\sigma_z^{(1)} \otimes \sigma_z^{(2)}$. To measure operators involving σ_y , we apply a transformation U that maps the eigenvectors of σ_y onto the eigenvectors of σ_z , i.e. $U\sigma_y U^{-1} = \sigma_z$, where $U = R(\pi/2, \pi)$. Similarly, the operator σ_x is transformed into σ_z by choosing $U = R(\pi/2, 3\pi/2)$. Therefore, all expectation values can be determined by measuring $\sigma_z^{(1)}$, $\sigma_z^{(2)}$ or $\sigma_z^{(1)} \otimes \sigma_z^{(2)}$. To obtain all 16 expectation values, nine different settings have to be used (see table I). Since a finite number of experiments allow only for an estimation of the expectation values $\langle \sigma_i^{(1)} \otimes \sigma_j^{(2)} \rangle_\rho$, the reconstructed matrix ρ_R is not guaranteed to be positive semi-definite[19]. Therefore, we employ a maximum likelihood estimation of the density matrix[19, 20], following the procedure as suggested and implemented in refs. [20, 21]. We parametrize the density matrix by the elements of the Cholesky matrix T related to ρ by $\rho = T^\dagger T$. Since the reconstructed density matrix ρ_R can have negative eigenvalues, we cannot use ρ_R as a starting point for the optimization routine. Instead, we use $\rho_P = P\rho_R P / \text{tr}(P\rho_R P)$ where P projects onto the subspace spanned by the eigenvectors of ρ_R having non-negative eigenvalues.

TABLE I: Additional pulses used for reconstructing a two-qubit quantum state. All expectation values needed for quantum state reconstruction can be determined by applying either one of the nine different transformations given in the table below and subsequently measuring the qubit state. Only the expectation values of the operators displayed in bold face are used to reconstruct the quantum state.

	Transformation applied to		Measured expectation values		
	ion 1	ion 2			
1	-	-	$\sigma_z^{(1)}$	$\sigma_z^{(2)}$	$\sigma_z^{(1)} \otimes \sigma_z^{(2)}$
2	$R(\pi/2, 3\pi/2)$	-	$\sigma_x^{(1)}$	$\sigma_z^{(2)}$	$\sigma_x^{(1)} \otimes \sigma_z^{(2)}$
3	$R(\pi/2, \pi)$	-	$\sigma_y^{(1)}$	$\sigma_z^{(2)}$	$\sigma_y^{(1)} \otimes \sigma_z^{(2)}$
4	-	$R(\pi/2, 3\pi/2)$	$\sigma_z^{(1)}$	$\sigma_x^{(2)}$	$\sigma_z^{(1)} \otimes \sigma_x^{(2)}$
5	-	$R(\pi/2, \pi)$	$\sigma_z^{(1)}$	$\sigma_y^{(2)}$	$\sigma_z^{(1)} \otimes \sigma_y^{(2)}$
6	$R(\pi/2, 3\pi/2)$	$R(\pi/2, 3\pi/2)$	$\sigma_x^{(1)}$	$\sigma_x^{(2)}$	$\sigma_x^{(1)} \otimes \sigma_x^{(2)}$
7	$R(\pi/2, 3\pi/2)$	$R(\pi/2, \pi)$	$\sigma_x^{(1)}$	$\sigma_y^{(2)}$	$\sigma_x^{(1)} \otimes \sigma_y^{(2)}$
8	$R(\pi/2, \pi)$	$R(\pi/2, 3\pi/2)$	$\sigma_y^{(1)}$	$\sigma_x^{(2)}$	$\sigma_y^{(1)} \otimes \sigma_x^{(2)}$
9	$R(\pi/2, \pi)$	$R(\pi/2, \pi)$	$\sigma_y^{(1)}$	$\sigma_y^{(2)}$	$\sigma_y^{(1)} \otimes \sigma_y^{(2)}$

For the pulse sequence that is designed to produce the state $\Psi_+ = (|10\rangle + |01\rangle)/\sqrt{2}$, we obtain the density matrix ρ_{Ψ_+} shown in Fig. 1a. The fidelity F of the reconstructed state is $F = \langle \Psi_+ | \rho_{\Psi_+} | \Psi_+ \rangle = 0.91$. To produce the state $\rho_{\Psi_-} = (|10\rangle - |01\rangle)/\sqrt{2}$, we change the phase of the sideband π -pulse by π and experimentally obtain the density matrix ρ_{Ψ_-} shown in Fig. 1b. For $\Phi_\pm = (|11\rangle \pm |00\rangle)/\sqrt{2}$, we find the density matrices depicted in Fig. 1c and d.

Having reconstructed a Bell state's density matrix, we can now check that the two qubits are indeed entangled. It has been shown that a mixed state ρ of two qubits is entangled if and only if its partial transpose ρ^{PT} has a negative eigenvalue[22, 23]. Not surprisingly, the partial transpose of the density matrix ρ_{Ψ_+} (Fig. 1a) has eigenvalues $\{-0.42(2), 0.40(2), 0.49(2), 0.53(3)\}$ close to the values of a maximally entangled state $\{-0.5, 0.5, 0.5, 0.5\}$. Errors in the determination of the density matrix elements and of quantities derived from them occur mainly as a consequence of quantum projection noise. Systematic effects like pulse length errors or addressing errors (coherent excitation of an ion by stray light) play a minor role. We estimate the magnitude of quantum projection noise by a bootstrapping technique [24] where the reconstructed density matrix serves for calculating probability distributions used in a Monte-Carlo simulation of our experiment.

Among the different measures put forward to quantify the entanglement of mixed bipartite states, the entanglement of formation, E , has the virtue of being analytically calculable from the density matrix of a two-qubit system. For a separable state, $E = 0$, whereas $E = 1$ for a maximally entangled state. Using the formula given by Wootters[25], we find $E(\rho_{\Psi_+}) = 0.79(4)$.

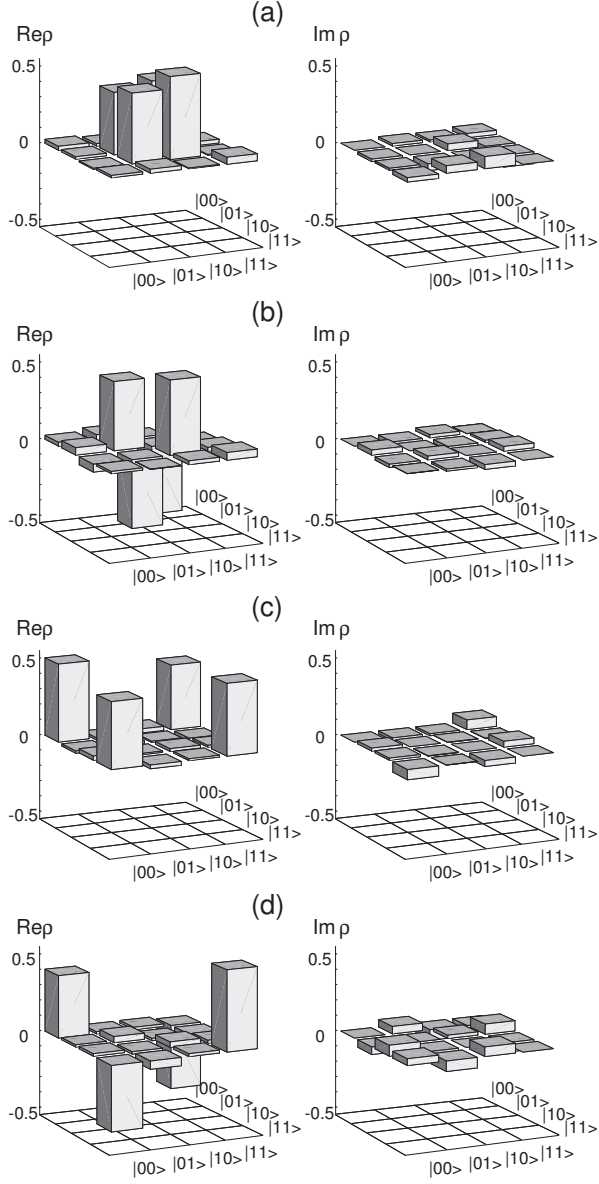


FIG. 1: (a): Real and imaginary part of the density matrix ρ_{Ψ_+} that approximates $\Psi_+ = (|10\rangle + |01\rangle)/\sqrt{2}$. The measured fidelity is $F_{\Psi_+} = \langle \Psi_+ | \rho_{\Psi_+} | \Psi_+ \rangle = 0.91$. (b): Real and imaginary part of the density matrix ρ_{Ψ_-} that approximates $\Psi_- = (|10\rangle - |01\rangle)/\sqrt{2}$. The measured fidelity is $F_{\Psi_-} = 0.90$. (c),(d): Density matrix elements of ρ_{Φ_+} (c) and ρ_{Φ_-} (d). Here, $F_{\Phi_+} = 0.91$ and $F_{\Phi_-} = 0.88$.

For the density matrices that nominally correspond to the Bell states Ψ_- and Φ_{\pm} , we measure $E(\rho_{\Psi_-}) = 0.75(5)$, $E(\rho_{\Phi_+}) = 0.76(4)$ and $E(\rho_{\Phi_-}) = 0.72(5)$.

All of these Bell states violate a Clauser-Horne-Shimony-Holt inequality. For the state ρ_{Ψ_+} , for example, we obtain $|\langle A \rangle| = 2.52(6) > 2$, where we have introduced the operator $A = \sigma_x^{(1)} \otimes \sigma_{x-z}^{(2)} + \sigma_x^{(1)} \otimes \sigma_{x+z}^{(2)} + \sigma_z^{(1)} \otimes \sigma_{x-z}^{(2)} - \sigma_z^{(1)} \otimes \sigma_{x+z}^{(2)}$, with $\sigma_{x\pm z} = (\sigma_x \pm \sigma_z)/\sqrt{2}$.

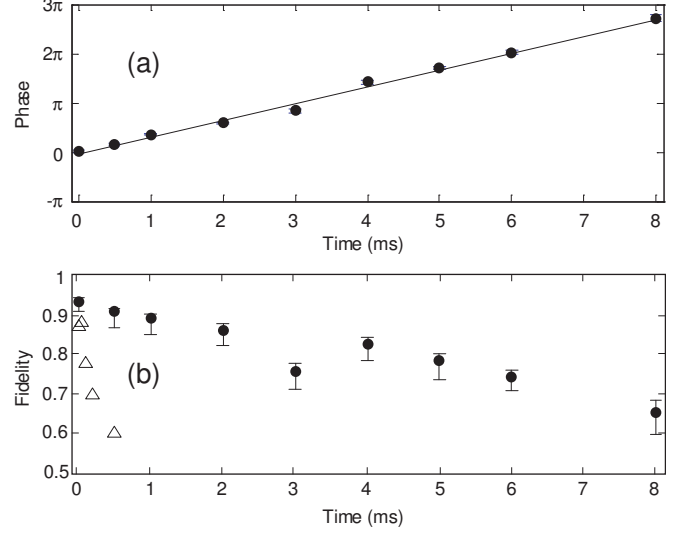


FIG. 2: Time evolution of the state $\Psi_+ = (|10\rangle + |01\rangle)/\sqrt{2}$. A magnetic field gradient causes the relative phase between the $|10\rangle$ and the $|01\rangle$ parts to evolve linearly in time. Decoherence leads to a loss of fidelity. (a) Phase $\beta_m(t)$ for which the overlap $F_m = \max_{\beta} (\langle \Psi_{\beta} | \rho_{\Psi_+}(\tau) | \Psi_{\beta} \rangle)$ between $\rho_{\Psi_+}(\tau)$ and states of type $\Psi_{\beta} = (|10\rangle + \exp(i\beta)|01\rangle)/\sqrt{2}$ is maximized. (b) Fidelity $F = \langle \Psi_{\beta_L}(t) | \rho(\tau) | \Psi_{\beta_L}(\tau) \rangle$ of the measured density matrix $\rho(\tau)$ that nominally corresponds to the state $\Psi_{\beta_L}(\tau) = (|10\rangle + \exp(i\beta_L)|01\rangle)/\sqrt{2}$ (filled circles). The state $\Phi_+ = (|11\rangle + |00\rangle)/\sqrt{2}$ (triangles) is sensitive to fluctuations of the laser frequency and the magnetic field. Thus, its decay occurs on a much shorter time scale. Error bars account for quantum projection noise as well as systematic errors in the reconstruction process. They are derived from a Monte-Carlo simulation.

Once a Bell state has been produced, we monitor its evolution in time by waiting for a time t before doing state tomography. We expect the Bell states Ψ_{\pm} to be immune against collective dephasing due to fluctuations of the magnetic field or the laser frequency[11]. However, they will only be time-invariant if the energy separation $\hbar\omega$ between the qubit states $|0\rangle$ and $|1\rangle$ is the same for both qubits. A magnetic field gradient that gives rise to different Zeeman shifts on qubits 1 and 2 leads to a linear time evolution of the relative phase between the $|01\rangle$ and the $|10\rangle$ component of the Ψ_{\pm} states. This is indeed the case in our experiments. We calculate the maximum overlap $F_m = \max_{\beta} (\langle \Psi_{\beta} | \rho_{\Psi_+}(\tau) | \Psi_{\beta} \rangle)$ between the density matrix $\rho_{\Psi_+}(\tau)$ and the states $\Psi_{\beta} = 1/\sqrt{2}(|10\rangle + \exp(i\beta)|01\rangle)$ as a function of time. The phase $\beta_m(\tau)$ for which the maximum overlap F_m is obtained is drawn in Fig. 2a. The phase changes linearly with time according to $\beta_L = \omega_{\beta}\tau$ with $\omega_{\beta} = (2\pi)170$ Hz, revealing the presence of a field gradient of $dB/dz = 0.6$ G/cm in the direction of the ion string that transforms a Ψ_+ state into a Ψ_- state within 3 ms and vice versa[26]. The decay of the Bell state into a mixed state leads to a slow

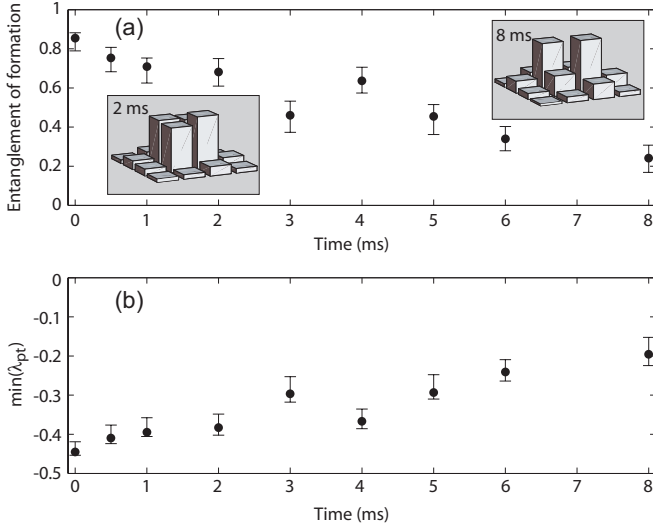


FIG. 3: Decay of the Bell state $\Psi_+ = (|10\rangle + |01\rangle)\sqrt{2}$ into a statistical mixture as a function of time. (a) Entanglement of formation and (b) smallest eigenvalue of the partial transpose of the density matrix. The insets show the magnitude of the density matrix elements measured after a time of 2 ms and 8 ms.

decline of the fidelity $F = \langle \Psi_{\beta_L} | \rho_{\Psi_+}(\tau) | \Psi_{\beta_L} \rangle$ over time which is shown in Fig. 2b. We find that the Ψ_{\pm} states decay into a statistical mixture within 5 ms whereas the Φ_{\pm} states already decay after about 200 μ s to a fidelity of $F = 0.75$. That decay can also be seen by drawing the entanglement of formation and the smallest eigenvalue of the partial transpose as a function of time as shown in Fig. 3. In some measurements, we found even longer lifetimes of the Ψ_{\pm} state approaching 20 ms.

With the methods demonstrated above we have deterministically created all four Bell states. State tomography yielded the complete information about the two-qubit quantum states. In future, this tomographic procedure will provide an efficient tool for evaluating quantum gates and the effect of decoherence in multi-qubit systems. We gratefully acknowledge support by the European Commission (QUEST and QGATES networks), by the Austrian Science Fund (FWF), and by the Institut für Quanteninformation GmbH.

- [2] D. T. Smithey, M. Beck, M. G. Raymer, A. Faridani, Phys. Rev. Lett. **70**, 1244 (1993).
- [3] T. J. Dunn, I. A. Walmsley, S. Mukamel, Phys. Rev. Lett. **74**, 884 (1995).
- [4] D. Leibfried, D. M. Meekhof, B. E. King, C. Monroe, W. M. Itano, D. J. Wineland, Phys. Rev. Lett. **77**, 4281 (1996).
- [5] Ch. Kurtsiefer, T. Pfau, J. Mlynek, Nature **386**, 150 (1997).
- [6] I. L. Chuang, N. Gershenfeld, M. G. Kubinec, D. Leung, Proc. R. Soc. London A **454**, 447 (1998).
- [7] A. G. White, D. F. V. James, P. H. Eberhard, P. G. Kwiat, Phys. Rev. Lett. **83**, 3103-3107 (1999).
- [8] A. G. White, D. F. V. James, W. J. Munro, P. G. Kwiat, Phys. Rev. A **65**, 012301 (2001).
- [9] E. Hagley, X. Maitre, G. Nogues, C. Wunderlich, M. Brune, J. M. Raimond, S. Haroche, Phys. Rev. Lett. **79**, 1 (1997).
- [10] Q. A. Turchette, C. S. Wood, B. E. King, C. J. Myatt, D. Leibfried, W. M. Itano, C. Monroe, D. J. Wineland, Phys. Rev. Lett. **81**, 3631 (1998).
- [11] D. Kielpinski, V. Meyer, M. A. Rowe, C. A. Sackett, W. M. Itano, C. Monroe, D. J. Wineland, Science **291**, 1013 (2001).
- [12] F. Schmidt-Kaler et al., Nature **422**, 408 (2003).
- [13] M. A. Nielsen, I. L. Chuang, Quantum Computation and Quantum Information (Cambridge Univ. Press, Cambridge, 2000).
- [14] Ch. Roos et al., Phys. Rev. Lett. **83**, 4713 (1999).
- [15] F. Schmidt-Kaler et al., J. Phys. B: At. Mol. Opt. Phys. **36**, 623 (2003).
- [16] H. Häffner et al., Phys. Rev. Lett. **90**, 143602 (2003).
- [17] Note that $|0\rangle$ and $|1\rangle$ are eigenvectors of σ_z corresponding to the eigenvalues +1 and -1, respectively.
- [18] U. Fano, Rev. Mod. Phys. **29**, **74** (1957).
- [19] Z. Hradil, Phys. Rev. A **55**, R1561 (1997).
- [20] K. Banaszek, G. M. D'Ariano, M. G. A. Paris, M. F. Sacchi, Phys. Rev. A **61**, 010304 (1999).
- [21] D. F. V. James, P. G. Kwiat, W. J. Munro, A. G. White, Phys. Rev. A **64**, 052312 (2001).
- [22] A. Peres, Phys. Rev. Lett. **77**, 1413 (1996).
- [23] M. Horodecki, P. Horodecki, R. Horodecki, Phys. Lett. A **223**, 1 (1996).
- [24] B. Efron, R. Tibshirani, Stat. Science **1**, 54 (1986).
- [25] W. K. Wootters, Phys. Rev. Lett. **80**, 2245 (1998).
- [26] The value of the field gradient was confirmed in an independent measurement.